JOURNAL OF GEOPHYSICAL RESEARCH, VOL. 104, NO. C7, PAGES 15,635–15,653, JULY 15, 1999

Rapid water exchange between the lagoon and the open ocean at Majuro Atoll due to wind, waves, and tide

Steven B. Kraines,[1] Atsushi Suzuki, [2] Tetsuo Yanagi, [3] Masahiko Isobe, [4] Xinyu Guo, [5] and Hiroshi Komiyama[1]

Abstract. Current measurements and conductivity-temperature-depth surveys of the lagoon and ocean at Majuro Atoll, the Republic of the Marshall Islands, were made from January 10 to 24, 1997. A vertically integrated tidal current model reproduced qualitatively well tidal ellipses calculated from the observed current measurements by Fourier transform. A three-dimensional, robust diagnostic residual current model explained the major features observed in the current measurements averaged over the dominant tidal cycles. We used the diagnostic model to examine the effects of wind stress, radiation stress, density gradients, and tidal stress on the exchange of water between the lagoon and the ocean. Wind effectively mixes the lagoon water in approximately 2 weeks. Tidal flushing appears to be restricted to a small area near the main channels connecting the lagoon to the ocean. Cross-reef-flat currents induced by radiation stress and flowing to the deep channels in the center of the northern boundary form the dominant mechanism for exchange between the lagoon and the open ocean, causing water to exchange completely with the ocean in about 15 days. Computer-generated particles tracked through the lagoon showed that radiation stress is also the main forcing mechanism for particle export from the lagoon. However, the coupling of tidal exchange through the Calalin Channel and wind-stress-induced mixing in the lagoon could also provide a significant export mechanism, particularly for particles originating uniformly inside the lagoon.

1. Introduction

The first step for any budgetary modeling of a coastal ecosystem is to analyze the exchange rates of the object of study with external sources and sinks of water. Often, a simple estimate of the residence time of a coastal marine ecosystem can be obtained from calculations based on the water budget and salinity gradients [*Gordon et al.,* 1996]. However, the goal of our study, to understand the changes that have occurred in the lagoon of Majuro Atoll as a result of the closure of the southern boundary and to evaluate various options to increase exchange of lagoon water with the ocean, requires a more interpretive analysis. In this paper we present the results of a modeling study of the currents at the lagoon of Majuro Atoll.

Several studies have been conducted on the circulation in the atolls of the Marshall Islands. *von Arx* [1948] investigated the contributions of wind, waves, tides, and the North Equatorial Current to the circulation in the lagoons of Bikini and Rongelap Atolls. On the basis of field surveys and scale models constructed in a laboratory, he calculated that the exchange time for oceanic water to replace the lagoon water at Bikini Atoll was approximately 39 days during the winter trade wind season and 80 days during the summer doldrums with similar values for Rongelap Atoll. The dominant source of oceanic water to the lagoon appeared to be wave-driven, cross-reef flow on the windward reefs. Wind stress caused water in the lagoon at Bikini Atoll to overturn once every 6.3 days in the winter and once every 12.5 days in the summer. Wave-driven, cross-reef flow is known to be an important mechanism for inducing circulation in coral reefs [*Tait,* 1972; *Symonds et al.,* 1995; *Hardy and Young,* 1996]. *Kraines et al.* [1998] describe the mechanism by which wave energy, which is

[1]Department of Chemical System Engineering, University of Tokyo, Tokyo.
[2]Marine Geology Department, Geological Survey of Japan, Tsukuba.
[3]Research Institute for Applied Mechanics, Kyushu University, Fukuoka, Japan
[4]Department of Civil Engineering, University of Tokyo, Tokyo.
[5]Institute for Global Change Research, Tokyo.

Paper number 1999JC900065.
0148-0227/99/1999JC900065$09.00

proportional to the square of the wave height, is converted to momentum flux, setup of the lagoon water level, and cross-reef currents in a coral reef. The excess momentum flux due to waves is termed radiation stress [*Longuet-Higgins and Stewart,* 1964].

Munk and Sargent [1948] showed that the conversion of wave momentum to surge currents on the windward coral reefs at Bikini Atoll resulted in a setup of the sea level on the reef flat of 0.6 m above both the ocean and the lagoon, which induces biologically important cross-reef currents. *Smith* [1973], in a study of a reef flat transect at Enewetak Atoll, observed that the flow across the windward reef flat was almost always into the lagoon. He observed volumetric flow rates of 0.04 to 0.60 m^3 s^{-1} m^{-1} reef flat near low tide, which corresponds to a current speed of about 10 to 120 cm s^{-1} for the 0.5 m deep reef flat. Dye released at the surface of the reef was observed to mix throughout the water column within 10 m of the point of release or about 1 to 10 s using the above cross-reef current speeds, indicating rapid vertical mixing on the reef flat. By determining the thickness of the stagnant boundary layer around the primary producers and thereby the rate of nutrient supply from the bulk water to the organism, *Bilger and Atkinson* [1995, 1992] and *Atkinson and Bilger* [1992] showed that the current speed of cross-reef flow may control reef flat production.

Ford [1949], using the radioactivity produced by the atomic bomb test on Baker Day, July 25, 1946, at Bikini Atoll, showed that a strong intrusion of oceanic water through the main channel displaced 40% of the lagoon water in 7 days. At this rate, the water in the lagoon of Bikini Atoll would exchange with the ocean in about 17 days. *Munk et al.* [1949] estimated vertical eddy diffusivity in the lagoon at Bikini Atoll from the relationship between wind speed and surface current velocity, vertical temperature profiles, and the mixing of reef water in the lagoon. All three methods gave vertical eddy diffusion coefficients of about 200 to 300 cm^2 s^{-1}. They estimated horizontal eddy diffusivity from radioactive tracers from the Baker Day bomb test to be about 1.5×10^5 cm^2 s^{-1} at the surface and 0.5×10^5 cm^2 s^{-1} at middepth.

Atkinson et al. [1981] studied the circulation at the lagoon of Enewetak Atoll. They also concluded that the major input of oceanic water was wave-driven inflow over the windward reef flat and measured cross-reef currents of up to 150 cm s^{-1}. Currents over the leeward reefs appeared to show a weak net outflow. Since the offshore mixed layer was over 73 m deep and the maximum channel depth is 56.7 m, only surface oceanic water entered the lagoon. The lack of stratification in the lagoon during their survey supported this hypothesis. However, despite the uniform density in the lagoon, they observed a distinct vertical current structure. Surface currents were primarily windward. An upwind return current occurred between the depths of 10 and 30 m with speeds about half the surface currents, and a deep flow traveled from the northeast windward reef flats to the south channel, where most of the water exited the lagoon. They concluded that wind-driven current is primarily restricted to internal circulation, in agreement with *von Arx* [1948]. Tides were important only within several kilometers of the channels. From estimates of the volume flows across the atoll boundaries, the lagoon residence time in winter was about 28 days.

Suzuki et al. [1997] measured salinity and carbonate parameters at Majuro Atoll in September 1994. Like *Atkinson et al.* [1981], Suzuki et al. found that the bottom of the surface mixed layer offshore was deeper than the sill of the deepest channel into the lagoon. In the lagoon, surface salinity increased from oceanic at 33.61 practical salinity units (psu) to 33.91 psu with distance from the windward reef flats. From the measurements of the carbonate parameters, they divided the atoll system into four water masses: offshore, east lagoon, west lagoon, and reef flat. The west lagoon values differed more from the offshore values than the east lagoon, so they concluded that the residence time was probably longer there. However, owing to the lack of strong salinity gradients and current measurements, they were unable to determine the residence time in the lagoon.

2. Study Site

Majuro Atoll is a part of the Ratak Archipelago in the Republic of the Marshall Islands, central Pacific Ocean. Majuro Atoll is located at 7°06'N and 171°12'E in the rain belt just north of the equator (Figure 1) and in the equatorial countercurrent. At the time of the survey, the strength of the northern equatorial countercurrent was estimated by the Japan Meteorological Agency from the geostrophic balance based on measurements of the spatial sea surface elevation to be of the order of 0.5 m s^{-1} . This area is also subject to strong trade winds from east-northeast during the winter, averaging about 7 to 8 m s^{-1} (Japan Meteorological Agency). The tidal type at Majuro Atoll $(M_2 + S_2)/(O_1 + K_1)$ is 5.8, indicating a dominance of the semidiurnal tidal cycle.

Majuro Atoll has a total area of about 393 km^2, with a total land area of about 15.9 km^2 and a reef flat area of 32.7 km^2 [*Suzuki et al.,* 1997]. Thus the lagoon consists of almost 90% of the total area. The maximum depth in the lagoon is 67 m, and the average depth is about 35 m, so the volume of the lagoon is about 1.2×10^{10} m^3. The atoll rim is well developed, and the southern boundary is completely landlocked except for a small passage in the SE corner of the atoll about 20 m wide and 3 m deep (Figure 2). All other openings along the southern boundary were filled to build a road. The increased closure of the lagoon at Majuro Atoll may be expected to result in a longer water residence time. The northern boundary of the atoll consists of shallow reef flats separated by sand cays. The main passage between the lagoon and the outer ocean is the Calalin

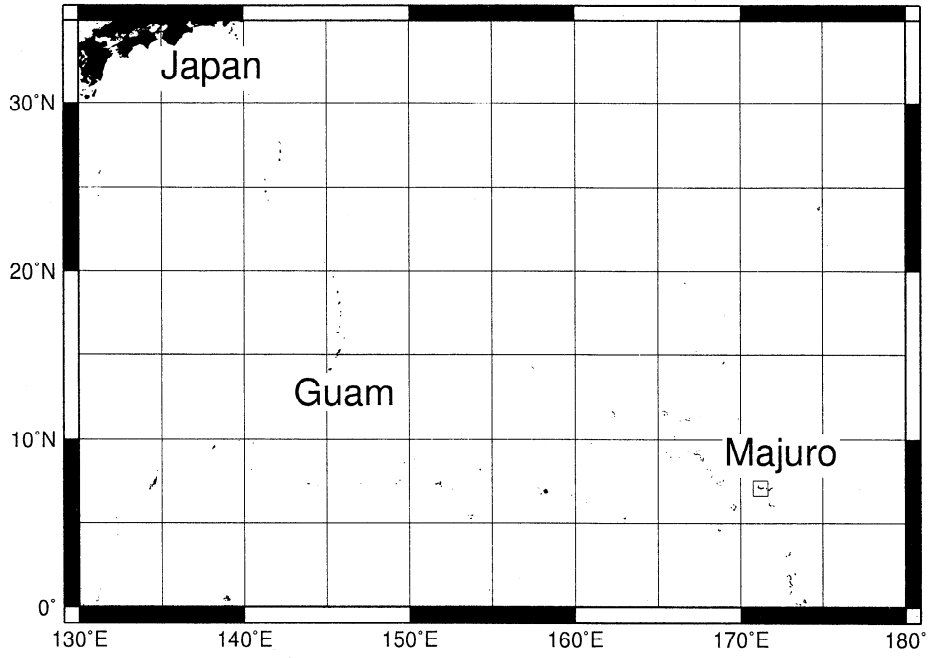

Figure 1. Area map showing the location of Majuro Atoll at 7°06'N and 171°12'E (rectangular region).

Channel, located at the center of the northern boundary with a maximum depth of 46 m. There is also a shallower channel to the west of the Calalin Channel with a maximum depth of about 20 m, hereafter termed the Western Channel. The east lagoon is relatively deep, while the west lagoon is shallower and has numerous coral knolls that reach close to the surface. Most of the 30,000 residents live on the eastern part of the atoll, so that the western half is relatively pristine.

3. Methods

We set three mooring lines at stations A, B, and C in the lagoon at depths of 50, 40, and 40 m respectively (Figure 2). On each line we attached an Aanderaa RCM-4 rotor-type current meter 10 m from the surface (precision, ±2%; detection limit, 2 cm s^{-1}) and an Alec Electronics ACM-8M electromagnetic-type current meter 10 m from the bottom (precision, ±2%; detection limit, 0.1 cm s^{-1}). The current meters were moored in the lagoon continuously from 1800 LT on January 9 to 1000 LT on January 24, covering the spring-neap tidal cycle. The mooring lines were supported by buoys fixed at 5 m depth, so the current meters should be free of influences from surface waves.

We also collected depth profiles of salinity and temperature at 17 locations in the lagoon and one site offshore of the Calalin Channel (Figure 2). For the first survey during the spring tide, we carried out conductivity-temperature-depth (CTD) casts at the lagoon sites on January 12 and at the offshore site on January 13. For the second survey during the neap tide, we carried out half of the casts on January 21 and the other half on January 22. CTD casts were made to the bottom at all sites in the lagoon and to a depth of 180 m at site 9 outside of the Calalin Channel. We used an Alec Electronics AST-1000 CTD profiler with precisions of ±0.05 psu for salinity, ±0.02°C for temperature, and ±1.1 m for depth.

We obtained meteorological data (precipitation and wind velocities) from the Majuro Weather Station, indicated by the triangle in Figure 2. Significant wave height data for the region over the survey period were provided by the Japan Meteorological Agency. High- and low-tide times and depths were obtained from the World Ocean Circulation Experiment (WOCE) database.

4. Observation Results

4.1. Wind and Precipitation

The meteorological data and tidal changes in sea level along with the survey period and the CTD cast times are shown in Figure 3. Wind velocities were fairly constant at 4 to 7 m s^{-1}, blowing in the direction of SW to W. Precipitation was generally less than 5 mm d^{-1}, with the exception of January 10 when 15 mm of rain fell and January 13 when more than 25 mm of rain fell. Significant wave heights varied between about 1.8 to 2.8 m during the survey period. The direction of offshore wave propagation was almost always toward west-southwest, i.e., generally the same as the wind direction.

4.2. Average (Residual) Currents

Current measurements showed a strong M_2 tidal component at the surface and bottom-moored meters at station C and smaller periodic oscillations at stations A

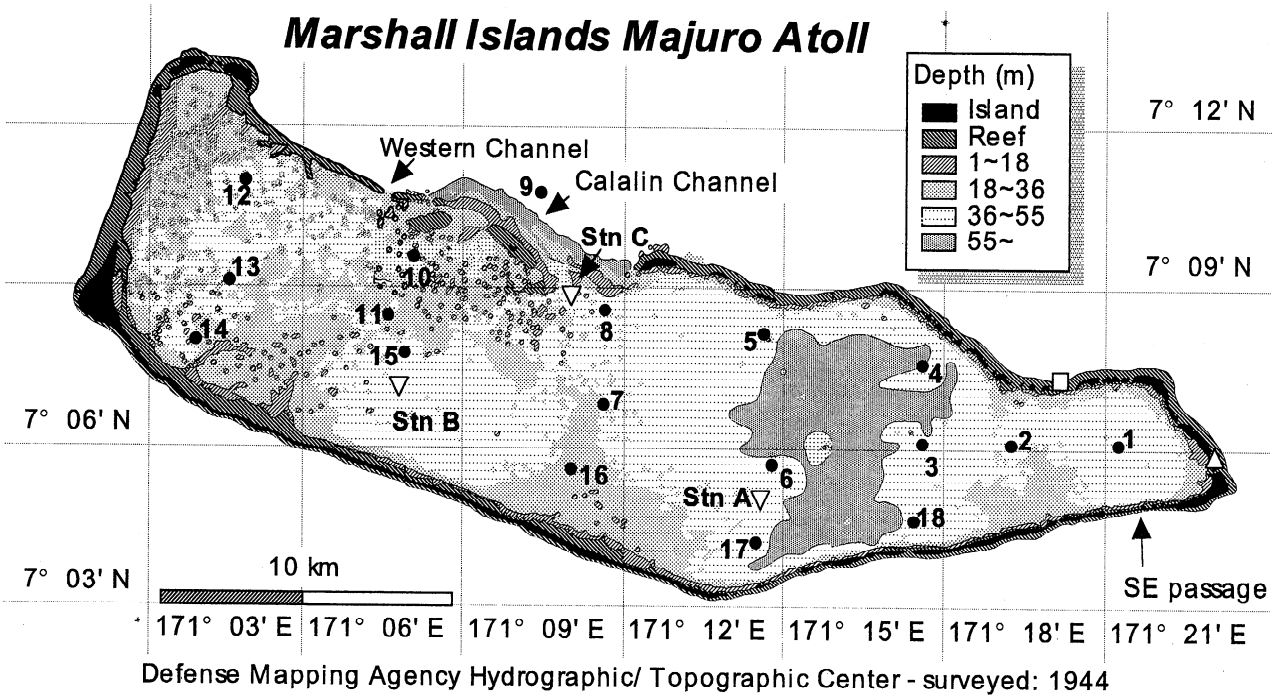

Figure 2. Locations of conductivity-temperature-depth (CTD) sites (circles) and mooring stations A, B, and C (inverted triangles). The locations of the Majuro Weather Station (triangle) and the reef flat station (square) are also shown. The Calalin Channel, the Western Channel, and the small boat passage in the southeast are indicated. The legend shows the depths for the different shadings. The unshaded area outside the atoll is at a depth of greater than 70 m.

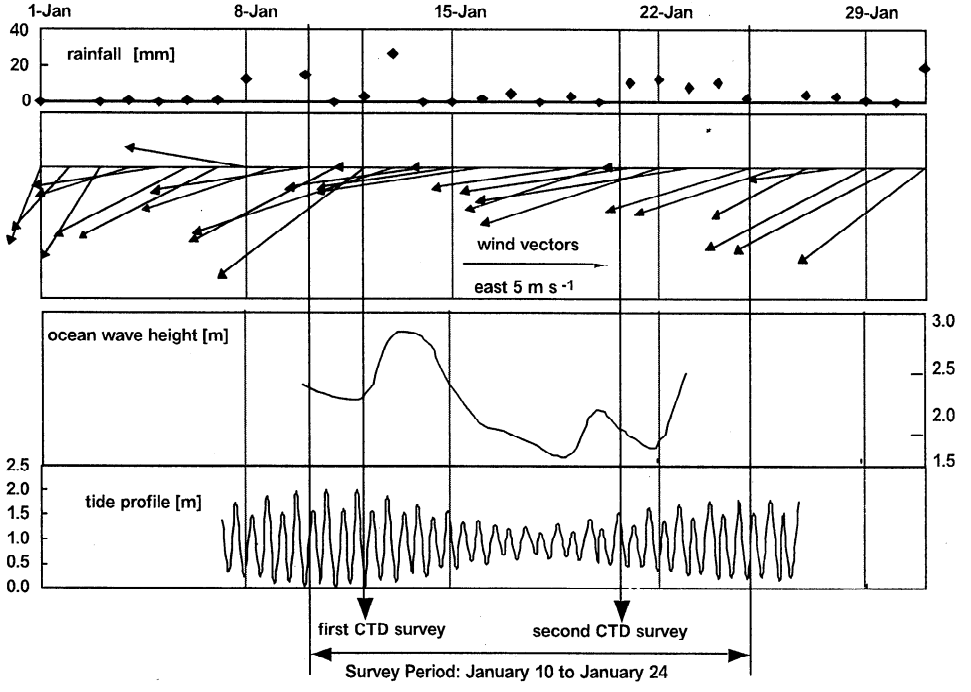

Figure 3. Weather observations at Majuro Atoll for the survey period. Daily average precipitation, wind vectors, significant ocean wave height, and the tide profile are shown. The survey period and the times of the CTD cast surveys are also indicated.

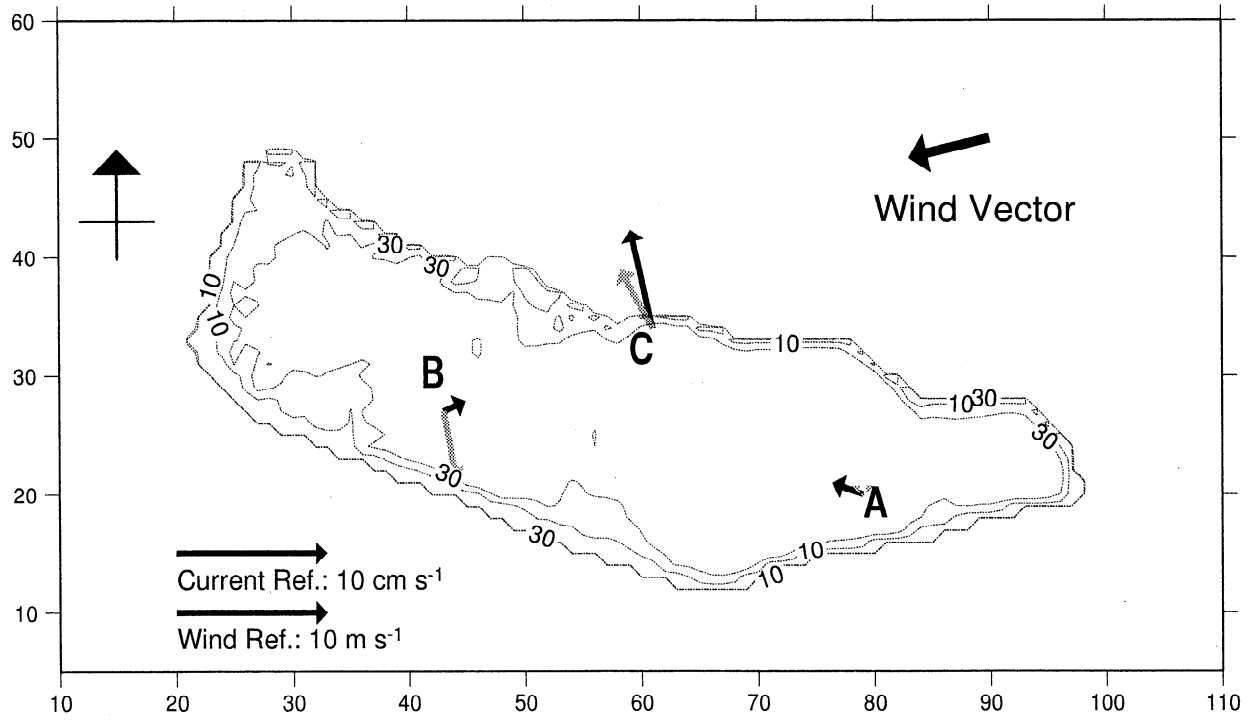

Figure 4. Average current vectors from current measurements 10 m from the surface (solid arrows) and 10 m from the bottom (shaded arrows) over the spring-neap tidal cycle. Average wind vectors for each day are also shown. The topography for the simulation is used to show depth contours. The x and y axes are the mesh numbers for the topographical database used by the model (i.e., units of 500 m). Reference vectors show a current speed of 10 cm s^{-1} and a wind speed of 10 m s^{-1}.

and B (not shown). The current vectors 10 m from the surface averaged over 28 cycles of the M_2 tide, i.e., approximately the M_2-S_2 spring-neap tidal cycle, show a flow pattern from the east and west lagoons through the Calalin Channel and out to the ocean (Figure 4). The average current vectors 10 m from the bottom are less clear. At station C, we observed a strongly barotropic flow directed to the north-northwest, i.e., out through the Calalin Channel. At station B, the average current 10 m from the bottom was directed toward the reef wall to the south.

From the average current exiting the lagoon through the Calalin Channel, the maximum turnover time for the water in the lagoon is 40 days. Application of the tidal prism theory results in a turnover time of 17 days [see *Suzuki et al.*, 1997], but most of this exchange is probably limited to the area close to the Calalin Channel. The strong outflow from the Calalin Channel in both the surface and bottom must be balanced by an inflow into the lagoon. The most likely mechanism is wind wave radiation-stress-driven flow over the windward reef flats.

4.3. Tidal Currents

We applied Fourier transforms for the M_2 and (K_1 + O_1) tidal components to an average 24.8 hour cycle with a 10 min sampling interval (each time step is averaged over the fourteen 24.8 hour cycles) to calculate tidal ellipses for each of the observed current profiles. Fourier analysis is simpler to apply than harmonic analysis and just about as effective for studying these tidal components.

Both tidal currents were strong at station C. While the tidal currents at stations A and B were less than 2 cm s^{-1}, the detection limit of the RCM meters, the surface and bottom ellipses at station C were aligned directly in and out of the Calalin Channel and were generally in phase (Figure 5). Close inspection of the daily variation in the M_2 and (K_1 + O_1) tidal ellipses shows a large day-to-day variability in the phases at stations A and B, so the phases and amplitudes of the tidal ellipses at those stations are not likely to be highly significant. The M_2 tidal ellipses at station C for the spring tide have the same direction as those for the neap tide but are almost 3 times as large (Figure 6), in agreement with the threefold difference between the spring and neap tidal ranges (see Figure 3).

We use these measurements to estimate the contribution of the tidal exchange in the Calalin Channel to the total tidal exchange required at Majuro Atoll by the tidal prism theory [*Prager*, 1991]. The total tidal exchange volume is the lagoon surface area times the av-

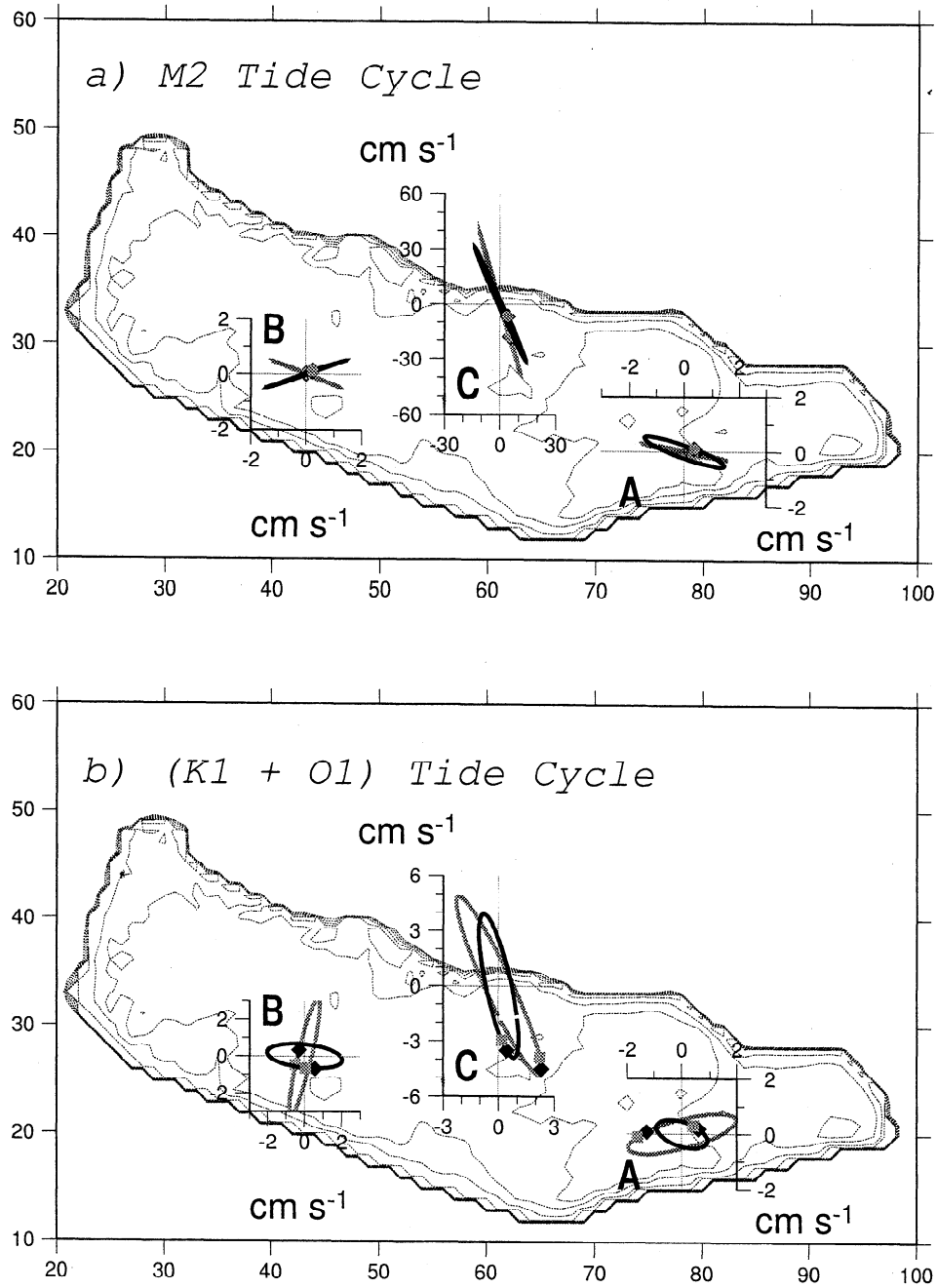

Figure 5. (a) M_2 and (b) (K_1 + O_1) tidal ellipses calculated by Fourier transform from the current measurements. Tidal ellipses are averaged over the spring-neap tidal cycle as explained in the text. Note the order of magnitude difference in the scales of the M_2 tidal currents at stations A and B and at station C. Diamonds and squares show the tidal currents at low tide and at 1 hour past low tide, respectively, indicating the direction of the change in tidal current. The definition of the (K_1 + O_1) tidal cycle is given in the text.

erage M_2 tidal range of 1.0 m or 3.8×10^8 m^3 per tidal cycle. The cross-sectional area of the Calalin Channel is approximately 39,000 m^2. The average tidal current is equal to the maximum current times $2\pi^{-1}$. From Figure 5a, the maximum M_2 tidal current at station C for the survey period is about 30 cm s^{-1}, yielding a tidal exchange through the channel of 1.7×10^8 m^3 per tidal cycle. Thus the tidal flow through the Calalin Channel accounts for roughly 45% of the tidal exchange at Majuro Atoll. The amplitude of the (K_1 + O_1) tide is only about 30% of that of the M_2 tide, and the tidal period is twice as long, so the (K_1 + O_1) tide should contribute little more than 10% of the tidal current, i.e., the tidal exchange at Majuro Atoll.

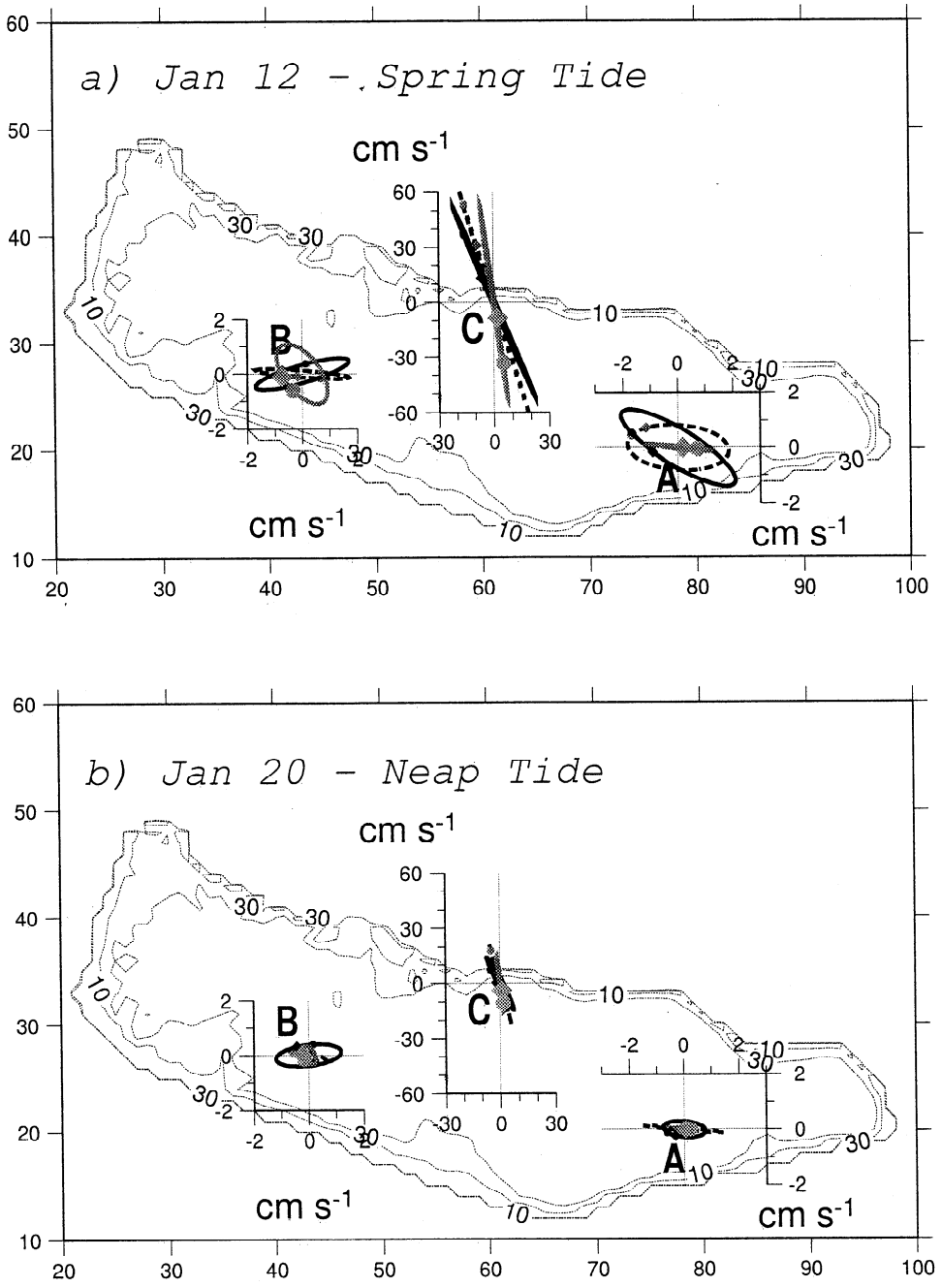

Figure 6. M_2 tidal ellipses for (a) January 12, 1997, showing results from the model forced by the M_2 spring tide, and (b) January 20, 1997, showing results from the model forced by the M_2 neap tide. Tidal ellipses calculated by Fourier transform from the results of the two-dimensional, vertically integrated tidal model for the M_2 tidal cycle are also shown.

4.4. CTD Profiles

None of the CTD depth profiles showed any strong indication of thermocline or halocline structure (Figures 7 and 8), in agreement with the observations of *Atkinson et al.* [1981] at Enewetak Atoll and of *von Arx* [1948] at Bikini Atoll. The lack of salinity gradient in spite of the relatively large precipitation at Majuro Atoll during the survey period indicates strong vertical mixing of the lagoon water. The largest differences between surface and bottom salinity appeared at sites 7 and 12. Site 7 is about 5 km from the Calalin Channel and may be within range of the tidal exchange through the channel. Site 12 is located in an area of relatively strong oceanic exchange across the reef flats to the east and west (Figure 2). Thus the larger salinity differences observed at these sites may be due to the direct influence of oceanic water.

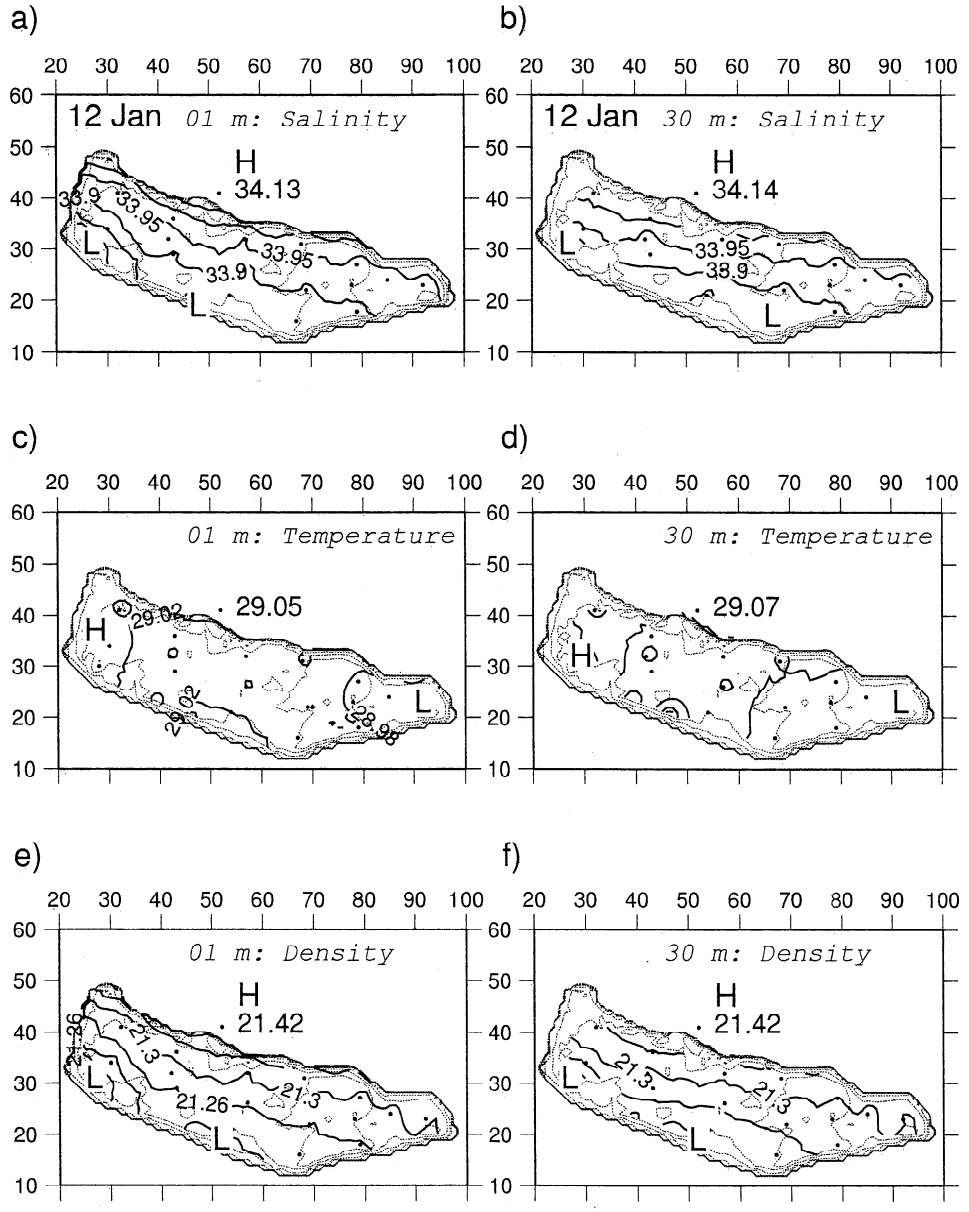

Figure 7. Salinity (psu) at (a) 1 m and (b) 30 m depth, temperature (°C) at (c) 1 m and (d) 30 m depth, and density at (e) 1 m and (f) 30 m depth on January 12, 1997. Salinity and temperature are from CTD casts. Density is calculated using the Knudsen state equation and shown in units of σ_T. Ocean values are shown with large numerals outside the atoll. Contour intervals are 0.05 psu for salinity, 0.04°C for temperature, and 0.04 kg m^{-3} for density. H indicates highs, and L indicates lows.

Spatial differences in the lagoon were also very small, indicating strong horizontal mixing. In the west lagoon, salinity and temperature decreased slightly near the SE island mass, possibly owing to a delayed input of freshwater from the fresh water lens under the island mass following the heavy rainfall on January 10 or to a longer water residence time in this region. Salinity and temperature were nearly uniform in the east lagoon, indicating the existence of a strong mechanism for mixing the lagoon water there.

On January 12, the surface salinity in the lagoon (33.77 to 33.96 psu) was significantly lower than that at site 9 on January 13 (34.13 psu), outside of the Calalin Channel (Figure 7a). This salinity difference may be due to the heavy rainfall that occurred on January 10 (Figure 3) or possibly to the timing of the CTD casts. As the tidal exchange is very important through the Calalin Channel, the CTD profiles at site 9 and the sites just inside the lagoon (CTD sites 8, 7, and 10) may be markedly different during ebb and flood tides. Site 9 was sampled during the middle of the ebb tide on January 13, while sites 7, 8, and 10 were sampled just before low tide on January 12. However, as the salinity throughout the entire lagoon should not change drastically over 1 day, the fact remains that there was a significant salinity difference between the inner lagoon and

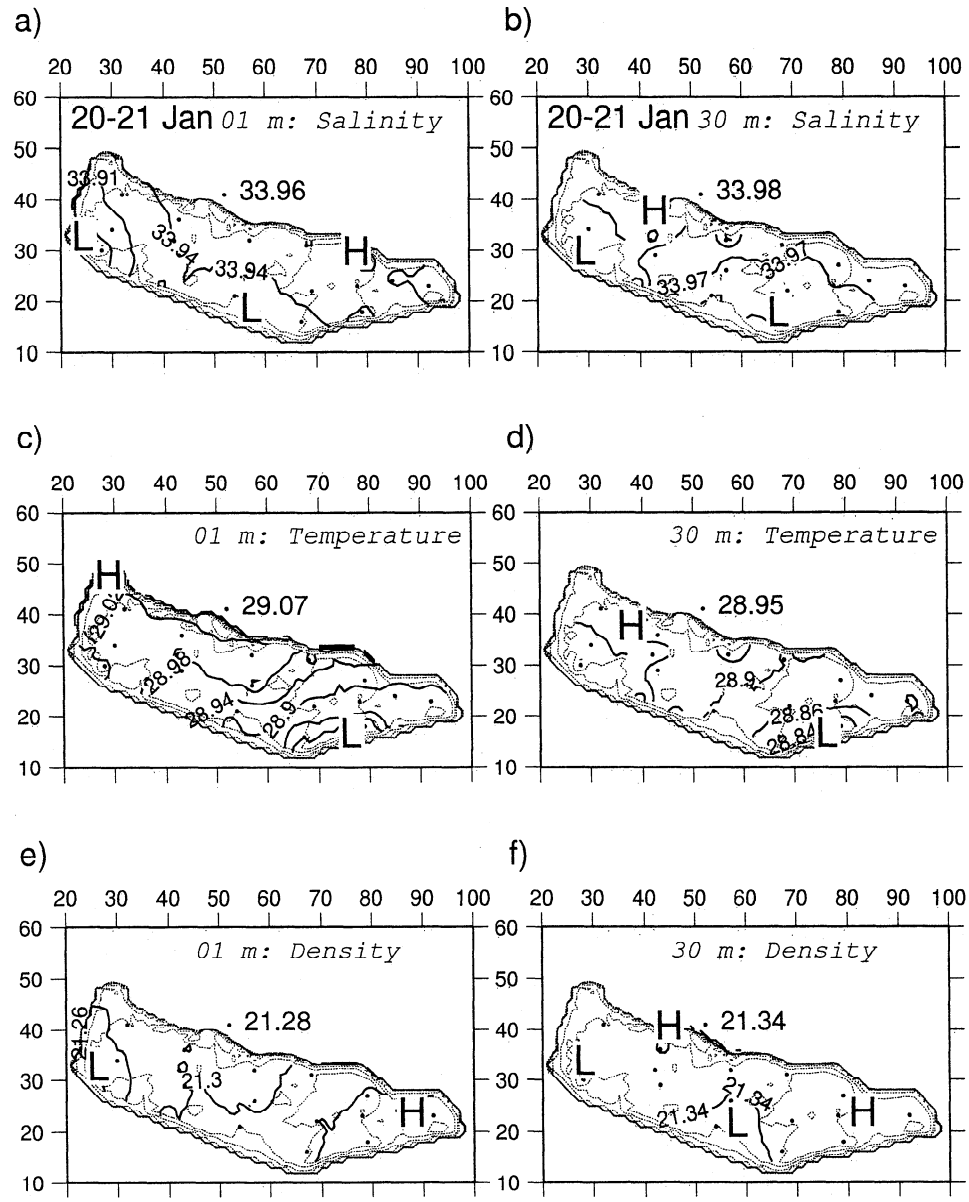

Figure 8. Same as Figure 7, but for January 20-21, 1997.

the ocean. Surface temperatures on January 12 were, in general, slightly lower in the lagoon than in the ocean. The air temperature varied from about 30°C at noon to 26°C at night. Thus the lower temperatures in the lagoon may be due to surface cooling. Bottom temperatures were less than or equal to surface temperatures except at sites 7 and 14 (Figures 7c and 7d). The increase of temperature with depth at site 7 supports the hypothesis that the bottom water at site 7 is, in fact, oceanic water entering into the bottom of the lagoon through the Calalin Channel.

On January 20-21, the difference observed on January 12 between the surface salinity in the lagoon and the ocean salinity measured at site 9 had disappeared (Figure 8a), mainly owing to a lowering of oceanic salinity. In the lagoon, surface and bottom salinities were lowest close to the southern island mass again (Figures 8a and 8b). A high in the bottom salinity occurred in the NW region of the lagoon (sites 8, 11, and 12). Temperature was again slightly lower in the lagoon. At sites 1, 7, and 12, bottom temperatures were higher than the surface (Figures 8c and 8d).

As temperature gradients were small during both surveys, density fields calculated from the observed temperature and salinity data from the Knudsen state equation generally reflected the same trends as the salinity fields (Figures 7e, 7f, 8e, and 8f).

5. Numerical Simulations of the Currents at Majuro Atoll

5.1. Numerical Simulations

Using a vertically integrated numerical simulation including tides, wind, and radiation stress, *Prager* [1991]

estimated the flushing period of a Caribbean-type back-reef lagoon to be less than 1 day. Computer-tracked drogues exited the lagoon in 6 to 10 hours. *Wolanski et al.* [1993] applied Prager's radiation stress formulation to study the flushing of pollutants from Tiahura Lagoon at Moorea, French Polynesia. They found that large waves resulted in strong flushing of the lagoon, but without the waves the currents were sluggish in the western lagoon, even in the presence of a strong trade wind. *Kraines et al.* [1998] applied a depth dependent formulation of radiation stress to a vertically integrated flow simulation to study the observed circulation in a small lagoon in the Ryukyu Islands of Japan. They were able to reproduce the temporal variations of the observed currents, and they calculated a residence time of computer-tracked particles in the lagoon of about 3 to 5 hours. *Wolanski and Pickard* [1983] studied the circulation and flushing of Britomart Lagoon, which is exposed to SE trade winds. They showed that the net outflow of 2.5×10^3 m^3 s^{-1} from the western channel must be supplied by an over-the-reef flow of at least 6 cm s^{-1}. By examining the balance between bottom friction and wind stress in the longshore direction and bottom friction and pressure gradients in the cross-shelf direction, they estimated the bottom friction coefficient to be 1.5 to 2.5×10^{-2}.

von Arx [1948] and *Atkinson et al.* [1981] pointed out that currents in atoll lagoons are driven by wind, waves, tides, and oceanic currents. In addition, differences in the effects of evaporation and precipitation in the shallow lagoon versus the deep ocean may induce density-driven currents between the lagoon and the ocean. *Atkinson et al.* [1981] noted that the very shallow perimeter reefs of the Marshall Island atolls isolate the lagoons from the influence of oceanic currents. A test run we carried out with a 0.5 m s^{-1} ocean current typical of the region resulted in little generation of currents within the lagoon. Therefore we model the effects of wind, waves, density, and tide on the circulation in the lagoon of Majuro Atoll.

We use two computer simulations to examine the effects of these driving forces. The first is a vertically integrated model forced by changing the elevation of the boundary meshes according to the observed major tide components and is identical to that used by *Kraines et al.* [1998] without radiation stress. The second is a three-dimensional diagnostic simulation adapted from the diagnostic model by *Guo and Yanagi* [1994, 1995, 1996, 1997], which includes the density-driven current, the wind-driven current, and the radiation-stress-driven, cross-reef transport. Both models are applied to a fine-scale realistic topography of Majuro Atoll with a mesh size of 500 m and run with a time step of 5 s, which is approximately equal to the Courant-Friedrichs-Lewy condition for a bottom depth of 100 m. Boundaries are taken to be at least 10 km from the atoll to avoid boundary effects on the modeled lagoon circulation.

The model equations for the three-dimensional diagnostic simulation are given by [*Guo and Yanagi*, 1997]:

$$\frac{\partial u}{\partial t} + \mathbf{u}\cdot\nabla u - fv = -\frac{1}{\rho_o}\frac{\partial P}{\partial x} + \frac{\partial}{\partial x}\left(A_h\frac{\partial u}{\partial x}\right) + \frac{\partial}{\partial y}\left(A_h\frac{\partial u}{\partial y}\right) + \frac{\partial}{\partial z}\left(A_v\frac{\partial u}{\partial z}\right) + F_{\text{rad stress}-x} + F_{\text{tidal stress}-x} \quad (1)$$

$$\frac{\partial v}{\partial t} + \mathbf{u}\cdot\nabla v + fu = -\frac{1}{\rho_o}\frac{\partial P}{\partial y} + \frac{\partial}{\partial x}\left(A_h\frac{\partial v}{\partial x}\right) + \frac{\partial}{\partial y}\left(A_h\frac{\partial v}{\partial y}\right) + \frac{\partial}{\partial z}\left(A_v\frac{\partial v}{\partial z}\right) + F_{\text{rad stress}-y} + F_{\text{tidal stress}-y} \quad (2)$$

$$\frac{\partial \eta}{\partial t}\frac{\partial}{\partial x}\int_{-h}^{0} u\,dz + \frac{\partial}{\partial y}\int_{-h}^{0} v\,dz = 0 \quad (3)$$

$$P = \rho_o g\,(\eta - z) + \rho_o g\int_z^0 \frac{\rho - \rho_o}{\rho_o}\,dz \quad (4)$$

Here Cartesian coordinates are used with the vertical coordinate directed upward and the horizontal coordinates laid out on the undisturbed sea surface; $\mathbf{u}$ is the three-dimensional velocity vector; ∇ is the gradient operator; t is time; u, v, and w are the x, y, and z components, respectively, of the residual velocity; A_h is the horizontal eddy viscosity; A_v is the vertical eddy viscosity; P is pressure; ρ is the density calculated from the CTD data using the Knudsen state equation; ρ_o is the average density; h is the undisturbed water depth; η is the sea surface elevation; f is the Coriolis parameter (8.469×10^{-5} s^{-1}); and g is the acceleration due to gravity. The F terms at the end of (1) and (2) denote forcing terms and will be discussed below. The equations are solved by the Alternating Direction Implicit (ADI) method as described by *Guo and Yanagi* [1994].

Two forcing terms, $F_{\text{tidal stress}}$ and $F_{\text{rad stress}}$, are included in (1) and (2). The tidal stress, $F_{\text{tidal stress}}$, is solved by integrating the harmonic results from the two-dimensional tidal simulation as described by *Guo and Yanagi* [1994]. The tide-induced residual flow from the tidal current is very small, except the region near the Calalin Channel, so we neglect it in the calculation of mean flow in the lagoon. $F_{\text{rad stress}}$ denotes the horizontal change in radiation stress per unit horizontal distance perpendicular to the reef flat and unit vertical distance through the water column. The x and y subscripts indicate the x- and y-directed components, respectively, of the stresses. We include the directional effect of waves that impinge on a reef flat that has varying normal vectors and the refraction effect of the waves as they refract to become more normal to the reef line by using the radiation stress tensor derived by *Longuet-Higgins and Stewart* [1964] and adapted by *Kraines et al.* [1998]. We used the wave heights from each of the

CTD survey periods (Figure 3) and the observed southwest direction of wave propagation.

The x- and y-directed $F_{\text{rad stress}}$ terms per unit vertical distance are calculated prior to the model run on all of the reef meshes using

$$F_{\text{rad stress}-x} = \frac{1}{h\,dx}\left(\frac{g}{8}\right) \left\{\left[n\left(1+\cos^2\theta\right)-0.5\right]\left(K_{\text{refract}}H\right)^2\right]_o - \left[n\left(1+\cos^2\theta\right)-0.5\right]H^2\Big]_{rf}\Big\} \quad (5)$$

$$F_{\text{rad stress}-y} = \frac{1}{h\,dy}\left(\frac{g}{8}\right) \left\{\left[n\left(1+\sin^2\theta\right)-0.5\right]\left(K_{\text{refract}}H\right)^2\right]_o - \left[n\left(1+\sin^2\theta\right)-0.5\right]H^2\Big]_{rf}\Big\} \quad (6)$$

$$K_{\text{refract}} = \sqrt{\frac{\cos\theta_o}{\cos\theta}} \quad (7)$$

Here n is the ratio of the group wave velocity to the wave celerity; H is the wave height; dx and dy are the x and y mesh widths, respectively; θ_o is the direction of the wave propagation in deep water, and θ is the direction of wave propagation near the reef, which differs from the deep water wave direction owing to the effect of refraction on the direction of the shoaling wave train. The wave direction θ is calculated using Snell's law as described by *Kraines et al.* [1998]. As the model calculates the steady state residual current, the radiation stress terms are kept constant following the initial calculation.

We revised the diagnostic simulation program to use fixed vertical levels of 50 cm, 1 m, 2, 5, 15, 25, 35, 45, 60, and 100 m for all meshes. As the minimum depth in the modeled regime is 1 m, each nonland mesh has at least two levels. The model was run for 2 days, upon which the total kinetic energy of the model regime calculated from the average current velocity became stable.

The boundaries, taken 10 km from the atoll, are closed for both simulations. We judged this method to be the most economical, considering that the lagoon is effectively isolated from the ocean currents by the atoll rim as described above and that the currents in the lagoon are forced mainly by processes in the lagoon and on the reef as we will describe below. As we observed the lagoon at Majuro Atoll to be vertically well mixed, constant vertical and horizontal eddy viscosity coefficients are justified. We set the horizontal eddy viscosity coefficient to the average of the surface and middepth values of the horizontal eddy diffusion coefficients obtained by *Munk et al.* [1949] for Bikini Atoll, i.e., 1×10^5 cm^2 s^{-1}. For the three-dimensional diagnostic model, the vertical eddy viscosity should be set smaller than the observed value, which is increased by wind mixing. We have used a value of 35 cm^2 s^{-1}, approximately one eighth the value given by *Munk et al.* [1949].

On the reef flat meshes (i.e., with depth less than 2 m), this eddy viscosity was not large enough to transfer the momentum flux due to bottom friction in level 2 to the water in level 1. We corrected this instability by increasing the eddy viscosity to 1000 cm^2 s^{-1} on the reef flat meshes, justified because the turbulent viscosity is believed to be far greater on the reef flats owing to the wave action as indicated by *Smith*'s [1973] observation of the rapid mixing of dye on the reef flat at Enewetak.

Wind stress and bottom friction stress are given by the following standard surface and bottom boundary conditions:

$$z = 0: \quad F_{\text{wind stress}} = C_d\rho_a\left(u_a, v_a\right)\sqrt{u_a^2+v_a^2} \quad (8)$$

$$z = -h: \quad F_{\text{bot stress}} = C_{br}\rho_o\left(u_b, v_b\right)\sqrt{u_b^2+v_b^2} \quad (9)$$

Here C_d is the nondimensional wind drag coefficient (1.3×10^{-3}), ρ is the density of air (1.2×10^{-3} g cm^{-3}), u_a and v_a are the wind velocity components, C_{br} is the drag coefficient of the seabed, and u_b and v_b are the velocity components above the seabed. In order to account for higher observed bottom frictions on reef flats with high bottom roughness, for meshes with depths 5 m or less we calculate C_{br} as a function of depth using Manning's formula [*Committee on Hydraulics*, 1985]. We set the Manning's coefficient to 0.10, the value used by *Kraines et al.* [1998]. For a depth of 1 m, the bottom friction coefficient is calculated to be 0.042, slightly larger than the values calculated by *Wolanski and Pickard* [1983]. At 5 m the bottom friction coefficient is 0.025. Below 5 m, we use a constant bottom friction coefficient of 0.0026.

The second term on the right side of (4) corresponds to the effect of density gradients on the momentum balance. The data from the CTD surveys were used to calculate the density stress field. We set all of the outside meshes equal to the profiles observed at site 9. In the lagoon, we used a distance-weighted average of the closest CTD sites to calculate temperature and salinity at each mesh. As the low salinities near the land masses are likely to result from delayed input of fresh water from the freshwater lenses of the land masses, we calculated hypothetical CTD profiles at the shore from linear extrapolation of each pair of shoreward directed CTD sites.

In order to account for the roughness of the CTD survey data, the model uses a robust diagnostic hydraulic computation [*Sarmiento and Bryan,* 1982; *Fujino and Imasato,* 1991]. The tendency for the temperature and salinity to remain close to the observed values is parameterized by a coefficient γ; that is, the standard diffusion-advection equation for heat transfer is weighted back to the observed profiles by γ. We ran

the model with values of γ ranging from (6 min) $^{-1}$ to (1 d) $^{-1}$, but the results did not differ markedly. For the runs described below, we set γ to be (30 min) $^{-1}$, which resulted in the best balance between a pure diagnostic simulation ($\gamma = \infty$) and an unweighted diffusion-advection simulation ($\gamma = 0$).

5.2. Depth-Integrated Tidal Current Simulation Results

The results of the model forced with a 1.5 m spring tidal range (M_2 + S_2) and a 0.5 m neap tidal range (M_2 - S_2) show that the strongest exchanges occur through the Calalin Channel and the Western Channel as predicted by the calculations from the observed data. The tidal ellipses plotted from the modeled currents are in reasonably good qualitative agreement with the observed tidal ellipses for the spring tide model, considering the weakness of the tidal currents at stations A and B (Figure 6a). Modeled tidal ellipses from the neap tide model run were considerably smaller than the spring tide model run and appeared to be smaller than the ellipses plotted from the observed data, particularly at stations A and B (Figure 6b). The magnitudes of the neap tide tidal currents at stations A and B were near the detection limit, so this discrepancy may be due to noise in the observations.

5.3. Three-Dimensional Robust Diagnostic Simulation Results

The residual surface flow field generated by the three-dimensional diagnostic model for the conditions of the first CTD survey (the model runs under the conditions of the CTD surveys on January 12, 1997, and January 20-21, 1997, are hereafter referred to as CTD1 and CTD2, respectively) shows strong cross-reef currents of up to 100 cm s^{-1} (Figure 9). These currents are generated by radiation stress due to waves breaking on the windward reef flats. Wind stress combined with density gradients in the lagoon result in a complex lagoonal circulation pattern. The surface circulations at 75 cm and 3.5 m depths are basically wind driven, although the density gradients in the west lagoon cause the flow to be directed to the SW. At 10 m, the current velocities are much smaller. Northward currents dominate the central lagoon, and an eastward current occurs in the west lagoon. The flow field at 30 m shows a relatively strong SE return flow in the western lagoon and a slight southern bottom flow just east of the Calalin Channel. Study of the circulations generated by running the simulation with density gradients only and wind stress only showed that the north-south components of the circulation can be explained almost entirely by the density field, while the only effect of the wind field below 5 m is

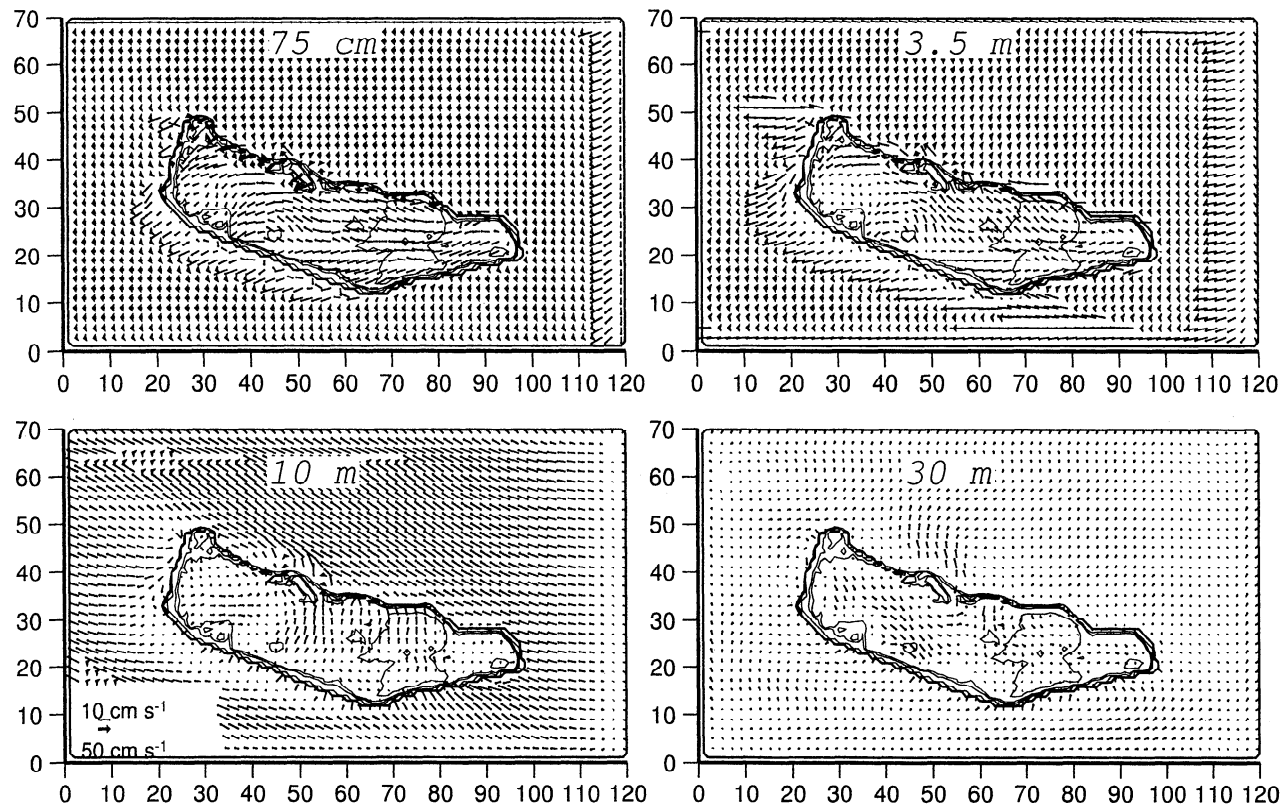

Figure 9. Results from the three-dimensional diagnostic residual current model using the temperature and salinity measurements and weather conditions from January 12, 1997. Flow fields at 75 cm, 3.5, 10, and 30 m are shown. Reference arrows in the lower left show current speeds of 10 and 50 cm s^{-1} for the two different arrow types.

in the eastern components of the flow in the west lagoon (data not shown).

Although there are some significant differences, simulation results from CTD1 and CTD2 qualitatively reproduce the major characteristics of the observed currents during each survey (Figures 10 and 11). In both simulations, the observed flow pattern 10 m below the surface is explained by radiation-stress-driven, cross-reef flow that enters the lagoon on the windward reef flats to the northeast and northwest and turns around toward the only major exit for water in the lagoon, namely, the Calalin Channel. There the water flows out strongly to the ocean, generally in agreement with the observed average current vectors at station C. On January 12, 1997, the larger wave heights result in a stronger outflow through the Calalin Channel and the currents at stations A and B are directed more northward than the observed vectors, apparently also a result of the stronger radiation stress effect (Figure 10a).

The observed current patterns 10 m from the bottom are also reproduced reasonably well by the modeled flow fields at 30 m depth. The radiation-stress-driven, cross-reef flow causes water to be driven out the Calalin Channel in the bottom layers as well as the surface in spite of the pronounced density gradient, particularly on January 12. On January 12, at station C the observed bottom average current had a strong western component not seen in the simulation results (Figure 10b). However, just outside the channel, the outward flow is met by an inward directed current vector (Figure 9), which is most likely an effect of the strong density gradient between the lagoon and the open ocean. With higher model resolution, the complex flow field at the channel may give rise to a flow at station C along the topography of the channel toward the open area to the west, which would result in a velocity in the observed current direction. This directional character in the bottom flow did not occur on January 20-21, and CTD2 showed a constant directional flow through the channel out to the ocean (Figure 11b).

The model predicts a strong return flow in the bottom currents at stations A and B, which differs from the observed current vectors. The southern flows observed in the bottom profile at station B are also not reproduced exactly, but the wind-driven eastern return flow is strongly deflected southward on January 12 and not on January 20-21, in agreement with the observations (Figures 10b and 11b). Considering that the major difference between the two surveys is the density field, the southern flow is most likely caused mainly by the density gradient near the southern island mass. The differences between CTD1 and CTD2 demonstrate the sensitivity of the simulation to wave height and density gradients.

In addition to the moored current meters in the lagoon, we also set up an ACM current meter on the reef flat at 171°20'E and 7°07'N (data not shown). The average cross-reef current speed measured there was 20 cm s^{-1}. The current speeds at that location predicted by CTD1 and CTD2 were 24 and 22 cm s^{-1}, respectively. For a model run with no radiation stress, the modeled current speed was just 1 cm s^{-1}.

From the temperature and salinity measurements of *Suzuki et al.* [1997] in September 1994 at Majuro Atoll, together with wave heights and wind speeds from that month obtained from the Japan Meteorological Agency, we calculated the flow field using the diagnostic simulation with the tidal stress field calculated from the spring tide tidal current model described above (hereafter CTD94). Although wind speeds were smaller in September 1994 than January 1997, resulting in more vertical structure of the CTD profiles in the lagoon [*Suzuki et al.*, 1997], wave heights around the atoll were slightly larger (Japan Meteorological Agency). As a result, the modeled flow exiting through the Calalin Channel that is driven by radiation-stress-induced, cross-reef flow was similar to the results obtained from the January 1997 survey data. However, the flow fields in the lagoon were substantially different from the previous runs, showing the strong effects of wind and density on the lagoon circulation.

6. Discussion

The flow fields simulated by the model runs show a combination of two strong circulation mechanisms. The strong winds during the survey period force a rapid circulation within the lagoon with modeled surface currents of the order of 10 cm s^{-1} and bottom return currents of 4 to 5 cm s^{-1}. The surface current carries water across the 40 km lagoon in 4.6 days; the bottom current returns this water to the eastern lagoon in about 10 days. Thus the wind-driven water turnover in the lagoon takes about 2 weeks. This period is somewhat longer than the estimate of *von Arx* [1948] for Bikini Atoll. The other strong circulation is the radiation-stress-driven flow from the reef flats to the channels in the center of the northern boundary of the lagoon. As we will demonstrate below, this radiation-stress-driven current appears to be the dominant mechanism exchanging water from the ocean, over the reef flats, into the lagoon, and back to the ocean through the deep channels.

In order to examine the effects of each of the forcing mechanisms, we conducted model runs with radiation stress only, wind stress only, density gradients only, and tidal stress only. From the flow fields generated by the three full-forced model runs described above and the simulation runs for each forcing term, we calculated the volume of seawater crossing the boundaries of the atoll as the sum of the lagoon-directed flow volumes across the atoll edge. The channels account for the bulk of the exchange, with the exchange through the small passage to the SE being negligible (Figure 12). We calculated

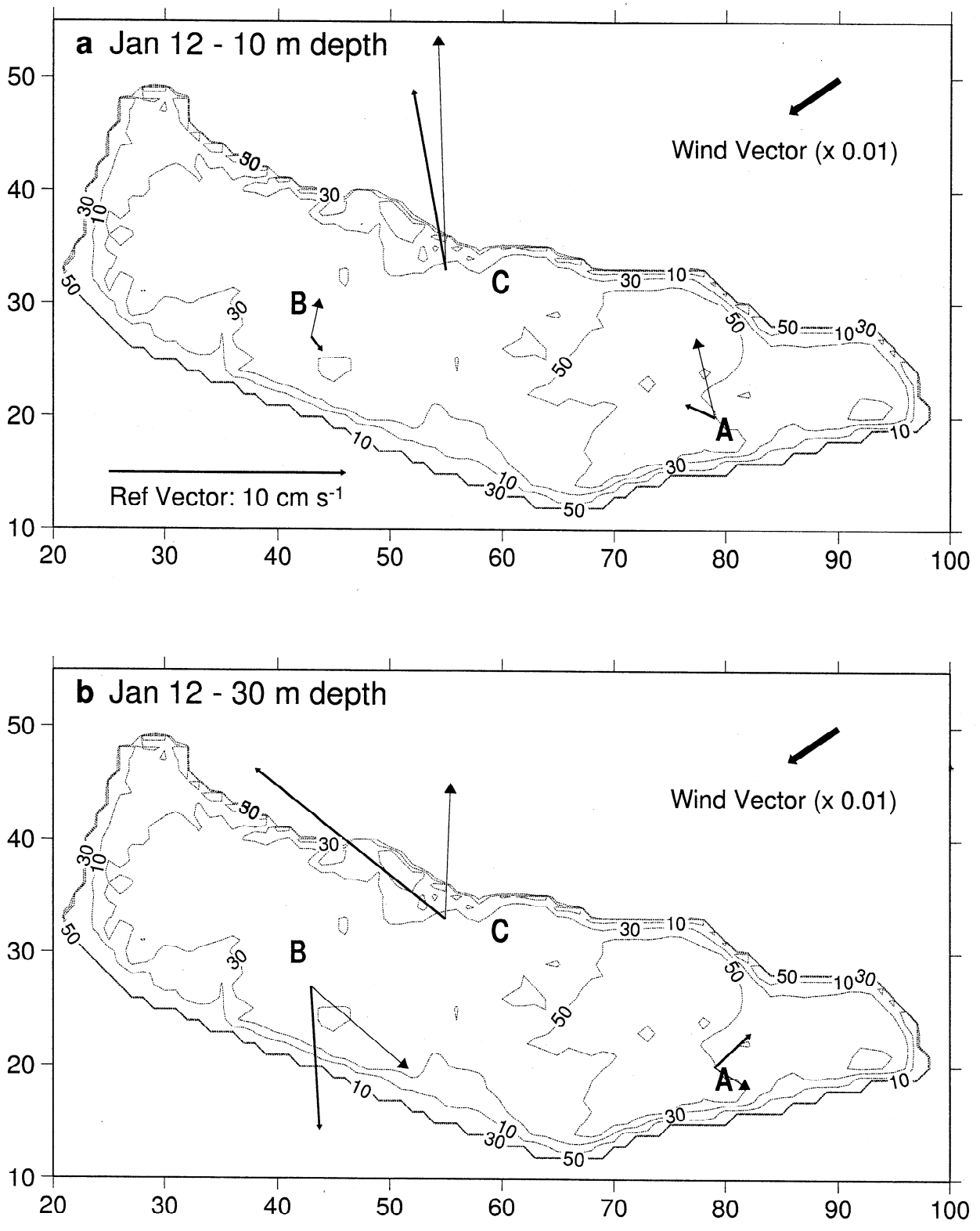

Figure 10. Comparison of the three-dimensional diagnostic residual current model results using the temperature and salinity measurements and weather conditions from January 12, 1997, with the average observed current vectors from the current meters moored 10 m from the surface and 10 m from the bottom, at (a) 10 m and (b) 30 m depth. Measured average current vectors are shown with thick lines and small heads; modeled current vectors are shown by thin lines and large heads. Wind vectors are shown at 0.01 times the length of the current vectors; that is, the reference vector of 10 cm s^{-1} is equivalent to a wind speed of 10 m s^{-1}.

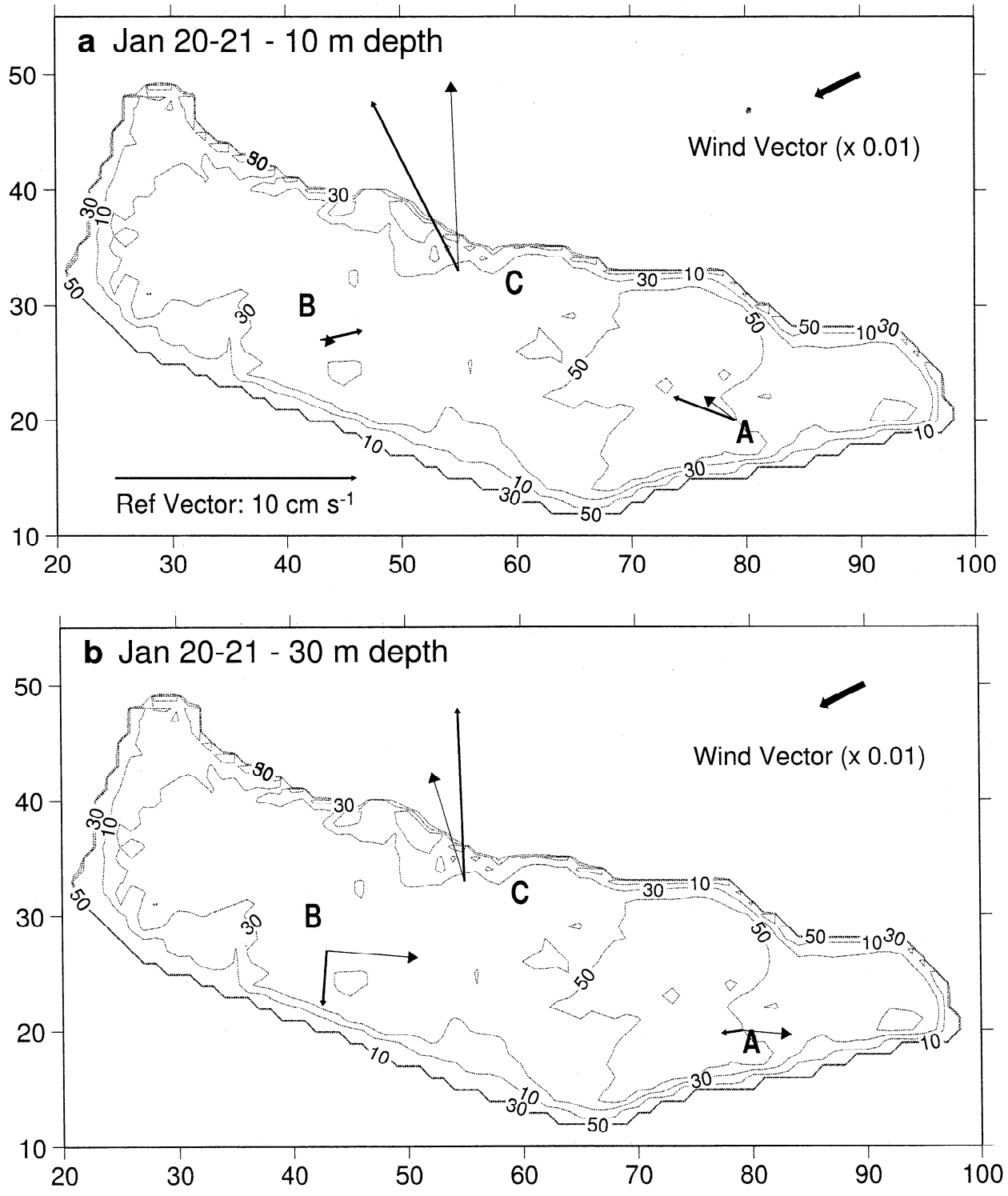

Figure 11. Same as Figure 10, but for model run using CTD data from January 20-21, 1997, and weather conditions from January 20, 1997.

the residence time τ in the lagoon as the lagoon volume divided by the outflowing seawater volume shown in Figure 12; that is,

$$\tau = \frac{\text{volume}}{\text{outflow rate}} \tag{10}$$

The residence times for each model run are shown on the right vertical axis scale in Figure 12 and summarized in Tables 1a and 1b. The model run forced by radiation stress on the reef flats with no wind or tidal stress and uniform density gradients resulted in an exchange volume almost the same as the CTD1 model run. The exchange volumes calculated from flow fields resulting from each of the other forcing terms were all less than 10% of the full forced exchange volumes (Tables 1a and 1b). Thus the exchange of seawater between the lagoon

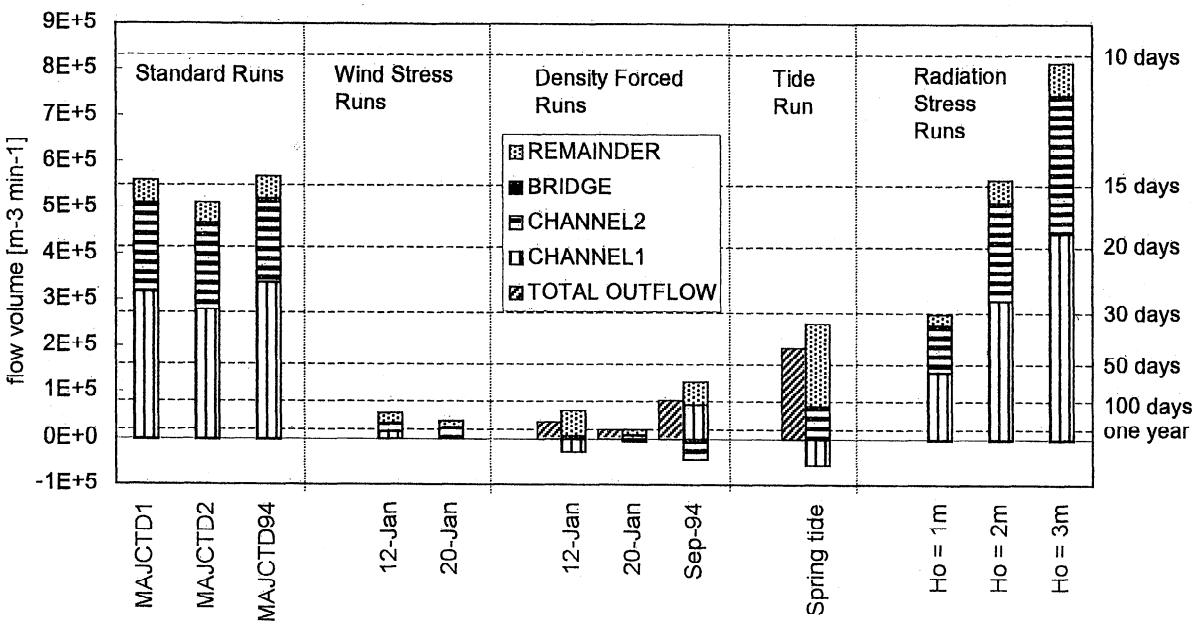

Figure 12. Bar graph showing the total seawater volume outflow across the atoll boundaries for each of the diagnostic model runs. Water residence times corresponding to the exchange volumes are shown at left. "Channel1" is the contribution of exchange through the Calalin Channel to the water exchange, "channel2" is the contribution of the Western Channel, "bridge" is the contribution of the SE passage, "remainder" is the exchange volume not accounted for by the above channels in the atoll boundaries. "Standard runs" are full forced model runs. "Wind stress runs" are forced with wind stress only. "Density-forced runs" are forced with density gradients only. The "tide run" is forced by tidal stress calculated from the depth-integrated tidal model run with the spring tide amplitude. "Radiation stress runs" are shown for ocean significant wave heights H_o of 1, 2, and 3 m. For cases where one of the channel flows is negative (inflow), the "total outflow" is given in dark shading.

and the ocean appears to be almost entirely controlled by radiation-stress-driven, cross-reef flow.

The residence times calculated here are smaller than most of the residence time estimates for Bikini Atoll and Enewetak Atoll described in the introduction. Test runs with openings in the southern boundary showed little change in the volume exchange rates; even relatively large openings on the leeward side simply redirected outflow from the lagoon away from the two main channels without changing the net outflow (data not shown). Apparently, the closure of the southern boundary of the lagoon does not affect the exchange of oceanic water appreciably since the cross-reef currents are still generated by radiation stress on the reef flats. *Kraines et al.* [1998] showed that radiation stress can result in rapid turnover of water in the lagoon of a small fringing reef. Previous methods of estimating the water residence time of coral reef lagoons may not have adequately accounted for the strong exchange mechanism of radiation stress on the windward reef flats.

We used the calculated flow fields to model the transport of particulate matter through the lagoon. Particles were tracked through the lagoon until either they came into contact with the seabed or they exited from the lagoon to the open ocean. Two cases were considered for each flow field. In the first case, particles were spread evenly throughout the lagoon both horizontally and vertically. In the second case, particles were set initially only in reef flat meshes (depth less than 2 m) to investigate the behavior of particles produced in those regions.

The equations for the particle tracking model are

$$X_{t+\Delta t} = X_t \mathbf{u}\Delta t + (\nabla \cdot \mathbf{u})\,\mathbf{u}\Delta t^2 + \mathrm{rand}\sqrt{2A_h\Delta t} \tag{11}$$

$$Z_{t+\Delta t} = Z_t + (w + w_s)\,\Delta t \tag{12}$$

Here X_t is the x, y position of the particle at time t, Z_t is the vertical position of the particle at time t, w_s is the sinking rate of the particle, $\mathbf{u}$ is the horizontal velocity of the particle, Δt is the time step of the particle model taken as 10 s, and rand is a random number from -1 to 1 used to parameterize the dispersion of the particles. The particle transport model was run for 50 days.

For all of the modeled cases, the majority of the particles sink within the lagoon (Tables 2a and 2b). This behavior may be overestimated by the model since particles that come into contact with the seabed may be

Table 1a. Water Residence Times Calculated From Flow Volumes Shown in Figure 12

	Standard Run	Wind Stress	Density Stress
Jan. 12, 1997	14.8	185	238
Jan. 20-21, 1997	16.3	270	552
Sept. 1994	14.7	N.A.	108

Units are in days. N.A. is not available.

resuspended into the water column. *Hata et al.* [1998] showed evidence for strong vertical fluxes of sinking particles at Palau. However, considering the rapid rate of decomposition of the particulate organic matter [*Martin et al.*, 1987; *Hata et al.*, 1998] as well as the sluggishness of the bottom flow field calculated here, the assumptions used in the model are probably sufficient to qualitatively estimate particle transport in the lagoon.

The results of the particle-tracking model are mainly useful for sensitivity tests. For both the lagoon origin case and the reef flat origin case, the largest export of particles from the atoll occurred using the flow field from the radiation-stress-driven model run. This export was even larger than that of the flow field generated by CTD1, implying that the interaction of the forcing terms may result in a damping effect on the advective export due to radiation stress.

The above results indicate that radiation-stress-driven, cross-reef currents are the dominant single mechanism forcing the export of particles from the lagoon to the open ocean at Majuro. Tidal exchange at Majuro Atoll produces a strong current through the deep channels on the northern boundary, but the limited duration of the tidal cycle precludes this exchange from being an important mechanism in exchanging lagoon water with the ocean beyond the immediate vicinity of the channels. Wind-forced circulation, while being an effective mechanism for keeping the lagoon well mixed, also does not result in much exchange with the open ocean. However, the two mechanisms when combined might result in a significant exchange.

In order to investigate this possibility, we tracked particles in the flow field resulting from the tidal model forced by the spring tide and determined the region around the channels where particles were exported during one M_2 tidal cycle. We then considered that particles in the three-dimensional tracking model that enter this region are immediately exported from the lagoon. The assumption here is that particles exiting the lagoon through the channels are swept away immediately by the offshore currents and therefore do not reenter the lagoon. The resulting contributions of this mechanism to the export of particles from the lagoon for the CTD1 and wind-only flow fields are shown in Table 2b. This mechanism results in a significant increase in export under both cases of particle origin compared to the full forced modeled flow field but still not quite as large as that using the radiation-stress-driven flow field in the reef flat origin case.

Table 1b. Water Residence Times For Radiation Stress Only Calculated From Flow Volumes in Figure 12

Wave Height, m	Residence Time, days
1.0	30.5
2.0	14.7
3.0	10.1

Table 2a. Results of the Reef-Flat Particle Trajectory Model Runs

Reef	Remain	Sink	Export
CTD1	30	58	12
CTD2	30	60	10
CTD94	33	63	4
CTD1*	20	51	28
CTD1†	37	54	9
	Wind Tide		
CTD1	28	50	22
	29†	48†	23†

Values are in percent.

"Remain" is the percentage of particles remaining in the water column of the lagoon, "sink" is the percentage of particles sinking to the bottom of the lagoon, and "export" is the percentage of particles exported from the lagoon to the open ocean. "Wind tide" indicates results including the wind-tidal exchange mechanism described in the text.

* Results were calculated from the first CTD survey with radiation stress only.

† Results were calculated from the first CTD survey with wind stress only.

Table 2b. Results of the Lagoon Particle Trajectory Model Runs

Lagoon	Remain	Sink	Export
CTD1	18	70	11
CTD2	18	72	10
CTD94	15	78	6
CTD1	20	52	29
CTD1	27	71	2
	Wind Tide		
CTD1	16	53	32
	23	44	33

See notes for Table 2a.

7. Conclusions

The distinct, unidirectional flow pattern from the east and west lagoons out through the Calalin Channel was explained by radiation-stress-induced flow over the windward reef flats at Majuro Atoll. Radiation stress was also shown to be the dominant factor in exchange of seawater with the open ocean and a major mechanism for flushing particulate matter from the lagoon to the open ocean. The forcing due to radiation stress is very sensitive to the open ocean wave height [*Kraines et al.*, 1998]. Current measurements just inside or directly on the windward reef flats combined with measurements of wave heights and wave directions outside of the atoll could provide a direct measure of this forcing.

The results from the survey conducted by *Suzuki et al.* [1997] in September 1994 showed that both vertical and horizontal salinity gradients were more pronounced at that time. Furthermore, in contrast with our survey results, they observed a salinity increase near the SE island mass. Thus the circulation in the lagoon during the summer doldrums might be thought to be weaker than the circulation we observed here. However, the results of the model run using data from that time period showed an even greater seawater exchange with the ocean than during our survey, attributed to the slightly larger wave heights during that period.

The particle-tracking model presented here is able to distinguish qualitatively between the behaviors of particle movement and export within the different flow fields calculated; however, a method is needed to verify the output from the model. Experiments with neutral buoyancy buoys and measurements of particle concentration distributions in the lagoon could help to quantify the results of the model.

Acknowledgments. We thank the Majuro local government, Ambassador Mack Kaminaga, and the Marshall Islands Marine Resource Authority for assistance in carrying out the fieldwork at Majuro Atoll and Robert Smith for providing us with background information that helped us to design the field survey. We owe the success of the field survey to the skilled work of Makoto Sasaki as well as the generous support of Tokyo Kyuei, Inc., and Sanyo Sokki, Inc. Hidetaka Takeoka and Yoshimi Suzuki provided helpful discussion concerning the interpretation of the observed data. The Japan Meteorological Agency and the Majuro Meteorological Agency provided valuable climate data for the simulations. This work was supported by the electric power companies of Tokyo, Kansai, Chubu, Kyushu, Tohoku and Okinawa, and their support is gratefully acknowledged. Finally, we thank two anonymous reviewers for their insightful critiquing of our manuscript.

References

Atkinson, M. J., and R. W. Bilger, Effects of water velocity on phosphate uptake in coral reef-flat communities, *Limnol. Oceanogr., 37,* 273-279, 1992.

Atkinson, M. J., S. V. Smith, and E. D. Stroup, Circulation in Enewetak Atoll lagoon, *Limnol. Oceanogr., 26,* 1074-1083, 1981.

Bilger, R. W., and M. J. Atkinson, Anomalous mass transfer of phosphate in coral reef flats, *Limnol. Oceanogr., 37,* 261-272, 1992.

Bilger, R. W., and M. J. Atkinson, Effects of nutrient loading on mass-transfer rates to a coral-reef community, *Limnol. Oceanogr., 40,* 279-289, 1995.

Committee on Hydraulics, Hydraulics formulae, 625 pp., Jpn. Soc. of Civ. Eng., Tokyo, Japan, 1985.

Ford, W. L., Radiological and salinity relationships in the water at Bikini Atoll, *Eos Trans. AGU, 30,* 46-66, 1949.

Fujio, S., and N. Imasato, Diagnostic calculation for circulation and water mass movement in the Deep Pacific, *J. Geophys. Res., 96,* 759-774, 1991.

Gordon, D. C., P. R. Boudreau, K. H. Mann, J.-E. Ong, W. L. Silvert, S. V. Smith, G. Wattayakorn, F. Wulff, and T. Yanagi, LOICZ Biogeochemical Modeling Guidelines, Publ. *LOICZ/ R&S/ 95-5,* 967 pp., LOICZ, Texel, Netherlands, 1996.

Guo, X., and T. Yanagi, Three dimensional structure of tidal currents in Tokyo Bay, Japan, *La Mer, 32,* 173-185, 1994.

Guo, X., and T. Yanagi, Wind driven current in Tokyo Bay, Japan during winter, *La Mer, 33,* 89-101, 1995.

Guo, X., and T. Yanagi, Seasonal variation of residual current in Tokyo Bay, Japan - Diagnostic numerical experiments, *J. Oceanogr., 52,* 597-616, 1996.

Guo, X., and T. Yanagi, Variation in residual current in Tokyo Bay due to increase of fresh water discharge, *Cont. Shelf. Res., 18,* 677-693, 1997.

Hardy, T.A., and I. R. Young, Field study of wave attenuation on an offshore coral reef, *J. Geophys. Res., 101,* 14,311-14,326, 1996.

Hata, H., A. Suzuki, T. Maruyama, N. Kurano, Y. Ikeda, S. Miyachi, and H. Kayanne, Carbon flux by suspended and sinking particles around the barrier reef of Palau, western Pacific, *Limnol. Oceanogr., 43,* 1883-1893, 1998.

Kraines, S. B., T. Yanagi, M. Isobe, and H. Komiyama, Wind wave driven circulation in the coral reef at Bora Bay, Miyako Island, *Coral Reefs, 17,* 133-143, 1998.

Longuet-Higgins, M. S., and R. W. Stewart, Radiation stresses in water waves: A physical discussion with applications, *Deep Sea Res., 11,* 529-562, 1964.

Martin, J. H., G. A. Knauer, D. M. Karl, and W. W. Broenkow, VERTEX: Carbon cycling in the northeast Pacific, *Deep Sea Res., Part A, 34,* 267-285, 1987.

Munk, W. H., and M. C. Sargent, Adjustment of Bikini Atoll to ocean waves, *Eos Trans. AGU, 29,* 855-860, 1948.

Munk, W. H., G. C. Ewing, and R. R. Revelle, Diffusion in Bikini Lagoon, *Eos Trans. AGU, 30,* 59-66, 1949.

Prager, E. J., Numerical simulation of circulation in a Caribbean-type backreef lagoon, *Coral Reefs, 10,* 177-182, 1991.

Sarmiento, J. L., and K. Bryan, An ocean transport model for the North Atlantic, *J. Geophys. Res., 87,* 394-408, 1982.

Smith, S. V., Carbon dioxide dynamics: A record of organic carbon production, respiration, and calcification in the Eniwetok reef flat community, *Limnol. Oceanogr., 18,* 106-120, 1973.

Suzuki, A., H. Kawahata, and K. Goto, Reef water CO_2 system and carbon cycle in Majuro Atoll, the Marshall Islands in the central Pacific, paper presented at 8th International Coral Reef Symposium, Smithson. Trop. Res. Inst., University of Panama, Balboa, Panama, 1997.

Symonds, G., K. P. Black, and I. R. Young, Wave-driven flow over shallow reefs, *J. Geophys. Res., 100,* 2639-2648, 1995.

Tait, R. J., Wave set-up on coral reefs, *J. Geophys. Res., 77,* 2207-2211, 1972.

von Arx, W. S., The circulation systems of Bikini and Rongelap lagoons, *Eos Trans. AGU, 29,* 861-870, 1948.

Wolanski, E., and G. L. Pickard, Long term observations of currents on the central Great Barrier Reef continental shelf, *Coral Reefs, 4,* 47-57, 1983.

Wolanski, E., B. Delesalle, V. Dufour, and A. Aubanel, Modeling the fate of pollutants in the Tiahura Lagoon, Moorea, French Polynesia, paper presented at 11th Australasian Conference on Coastal and Ocean Engineering, Sheraton Breakwater Hotel, Townsville, Australia, 1993.

X. Guo, Institute for Global Change Research, SEAVANS North 7F, 1–2–1 Shibaura, Minato-ku, Tokyo 105-6791 Japan. (guoxinyu@frontier.esto.or.jp)

M. Isobe, Department of Civil Engineering, University of Tokyo, 7–3–1 Hongo, Bunkyo-ku, Tokyo 113 Japan. (isobe@coastal.t.u-tokyo.ac.jp)

H. Komiyama and S. B. Kraines, Department of Chemical System Engineering, University of Tokyo, 7–3–1 Hongo, Bunkyo-ku, Tokyo 113 Japan. (steven@prosys.t.u-tokyo.ac.jp; komiyama@chemsys.t.u-tokyo.ac.jp)

A. Suzuki, Marine Geology Department, Geological Survey of Japan, 1–1–3 Higashi, Tsukuba 305-8567 Japan. (a_suzuki@gsj.go.jp)

T. Yanagi, Research Institute for Applied Mechanics, Kyushu University, 6–1 Kasuga-Park, Kasuga, Fukuoka 816-8580 Japan. (tyanagi@riam.kyushu-u.ac.jp)

(Received June 8, 1998; revised December 11, 1998; accepted January 25, 1999.)